A Photonic Electro-Optic Circuit for On-Chip Quantum Frequency Processing

by

Benjamin Nussbaum

Supervised by Doctor Joseph Lukens[*] and Professor A. Nick Vamivakas[†]

[*]Quantum Information Science Group, Oak Ridge National Laboratory, Oak Ridge, Tennessee

[†]The Institute of Optics, University of Rochester, Rochester, New York

The Institute of Optics
Hajim School of Engineering and Applied Sciences
School of Arts and Sciences

University of Rochester

Rochester, New York

2021

Contents

Contents ii

List of Figures iii

1 Background 4

1.1 Frequency encoding 5

1.2 Quantum information - the Hadamard gate 5

1.3 Integrated photonics 8

1.3.1 Micro-ring resonators 9

1.3.2 M-mode pulse shaper on-chip 10

2 Methods 11

2.1 Fidelity calculations 11

2.2 Log-fit to phase modulator data 12

3 Problems and progress 13

3.1 A realistic driving voltage model 13

3.2 Waveguide doping modification 14

4 Conclusion 16

5 Funding 16

6 Acknowledgements 16

References 17

List of Figures

1 A non-quantum example of optical frequency encoding. 5
2 Ideal EOM response to a sinusoidal driving voltage. 6
3 Ideal pulse shaper phase shifts for single Hadamard gates. 6
4 Ideal pulse shaper phase shifts for parallel Hadamard gates. 7
5 Comparison of existing laboratory setup and an integrated photonic chip. 8
6 Schematic diagram of a photonic micro-ring resonator. 9
7 Schematic diagram of an M-mode pulse shaper. 10
8 Pulse shaper output used to compute fidelity. 11
9 Logarithmic fit to phase modulator data and comparison with the ideal case. 12
10 Dependence of V_1 on V_{dc} for optimal gate fidelity. 12
11 Effects of a realistic driving voltage model on possible peak fidelity. 13
12 Parameter sweep over semiconductor doping in the EOM. 14
13 Fidelity and success probability with original and modified dopings. 15
14 EOM phase shift and attenuation with original and modified dopings. 15

1 Background

Classical, i.e. non-quantum, computers manipulate classical bits which may hold only one of two values—0 or 1—at any given time to perform calculations. Quantum computers work with quantum bits or 'qubits' which are not limited to single values, but can take on more complex states such as a superposition between the analogous values for a classical bit $|0\rangle$ and $|1\rangle$. As classical computational power grows, some problems continue to remain impractical to solve at large scales, becoming intractable for any typical use case. By leveraging knowledge of quantum interactions, recent algorithms promise efficient alternatives to the limited classical solutions.

However, before any quantum devices can have a chance of emulating the growth of classical computers, the technology must be scalable, efficient, and affordable. Although quantum information processing and quantum computing have been well established as fields of significant research interest, efforts to make these technologies scalable still pose significant challenges. While efforts to instantiate quantum computers by several methods have had varying degrees of success, existing systems are error-prone, can require elaborate cooling systems to keep the devices close to absolute zero, and are comprised of bulky, expensive components which contribute significant loss to the system. The field has no doubt come a long way, but growing beyond the present noisy intermediate scale quantum or 'NISQ' level will require new innovations and creative thinking.

Rather than following this same path of atom or electron spin to build qubits, or even exploring other properties of light such as polarization or spatial modes, encoding information in the wavelength or frequency of light supports a swath of potential advantage. This thesis will explore the use of a frequency mode space for quantum information processing in the mature platform of silicon photonics, focusing on the fundamental operation of a Hadamard transformation.

1.1 Frequency encoding

Apart from the benefit of being conceptually intuitive (figure 1 shows a simple example), frequency encoded information has been used for decades in the telecom industry, and many common components such as optical fibers, tuneable lasers, and spectrum analyzers are commercially available. The existing global optical fiber network could allow easily scalable quantum communication if cheap quantum devices using optical frequency to encode information can be developed.

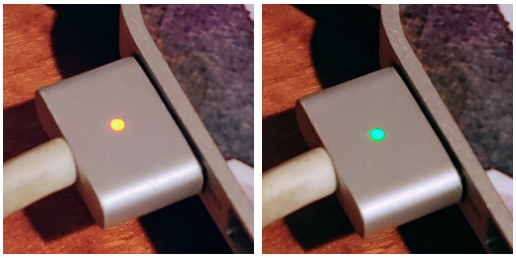

Figure 1: A (non-quantum) example of information encoded with optical frequency (wavelength). Left: an orange LED indicates that the laptop battery is charging and has not yet reached capacity. Right: a green LED indicates that the laptop battery is fully charged.

1.2 Quantum information - the Hadamard gate

Quantum logic gate operations are central to quantum computing and quantum information processing. Equation (1) shows two equivalent mathematical representations of the Hadamard transform, which is used in many quantum computing algorithms.

$$\hat{H} \triangleq \frac{|0\rangle + |1\rangle}{\sqrt{2}} \langle 0| + \frac{|0\rangle - |1\rangle}{\sqrt{2}} \langle 1| \qquad \Longleftrightarrow \qquad H_1 = \frac{1}{\sqrt{2}} \begin{bmatrix} 1 & 1 \\ 1 & -1 \end{bmatrix} \tag{1}$$

The process for applying a Hadamard transformation can be conceived as an arbitrary[1] operation:

1. Interfere or "mix" the modes of an input among constituent modes of the computation space.
2. Apply phase shifts on a per-mode basis.
3. Invert the coherent mode mixing operation to recombine and form an arbitrary output state.

For a Hadamard gate in a frequency mode space, this procedure can be implemented by sandwiching a pulse shaper (PS), which applies per-mode phase shifts, between two electro-optic modulators[2] (EOMs), which allow for coherent frequency mixing.

[1] By modifying the mode interference parameters and the phase shifts applied, any arbitrary transformation can be applied to a certain configuration of modes comprising an input state.

[2] An EOM modifies the refractive index of a material, and therefore the phase accumulated by a beam of light that passes through it, based on the electric voltage applied.

The EOM phase shift applied is dependent on the driving voltage over a cycle. The spacing between adjacent frequency modes $\Delta\omega = \frac{1}{T}$ is determined by the period[3] T of the EOM driving voltage. The ideal[4] EOM response for a Hadamard gate is shown in figure 2. The ideal phases

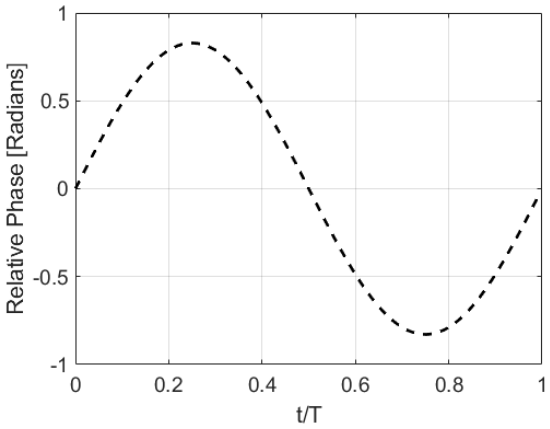

Figure 2: Ideal EOM response to a sinusoidal driving voltage. For use in conjunction with a pulse shaper, the period T determines the mode spacing such that $\Delta\omega = \frac{1}{T}$.

applied by the pulse shaper are shown in figure 3 for six and twelve modes. The Hadamard operator H defined in equation (1) would be applied to modes ω_2 and ω_3 or ω_5 and ω_6 with a varying number of guard-band modes in these cases. The label ω_m is used here to indicate that each mode corresponds to a particular optical frequency, though in general a Hadamard gate may operate via any arbitrary space on quantum or classical states.

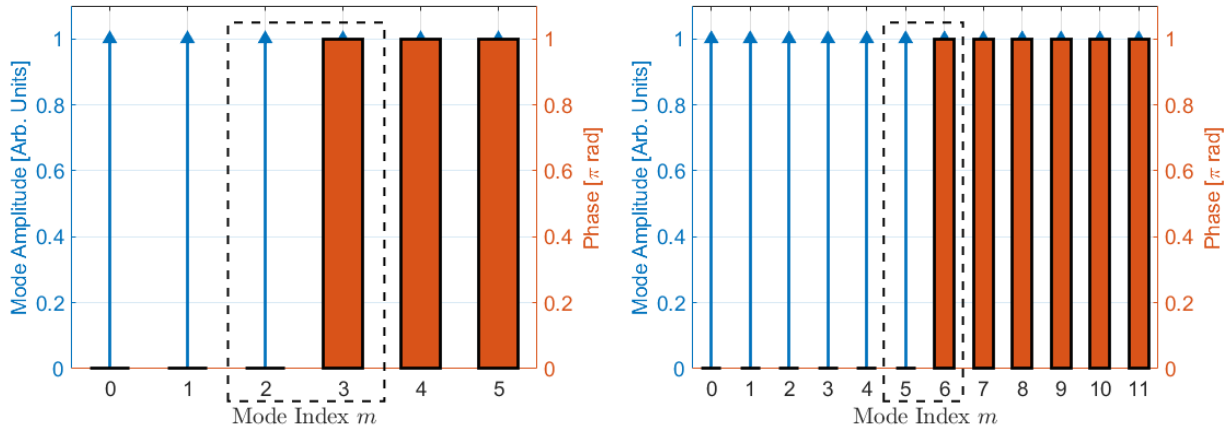

Figure 3: Ideal pulse shaper phase shifts for a 6-mode (left) and 12-mode (right) Hadamard gates. In each case, dashed boxes outline the logical modes.

[3]The driving voltage frequency can vary to determine the mode spacing, but variation on the order of e.g. 20 GHz is not a bad assumption.

[4]Ideal in this case refers to the maximum theoretical fidelity of the gate, see Lukens and Lougovski [4]

In the interest of increasing the information density of a given operation, it is useful to perform Hadamard transforms in parallel via equation (2), e.g. on computational mode pairs ω_2-ω_3 and ω_8-ω_9 for the 12-mode space ω_0-ω_{11} as shown in figure 4.

$$H_{\parallel}\left|\psi\right\rangle = \frac{1}{\sqrt{2}}\begin{bmatrix} 1 & 1 & 0 & 0 \\ 1 & -1 & 0 & 0 \\ 0 & 0 & 1 & 1 \\ 0 & 0 & 1 & -1 \end{bmatrix}\begin{bmatrix} \omega_2 \\ \omega_3 \\ \omega_8 \\ \omega_9 \end{bmatrix} \tag{2}$$

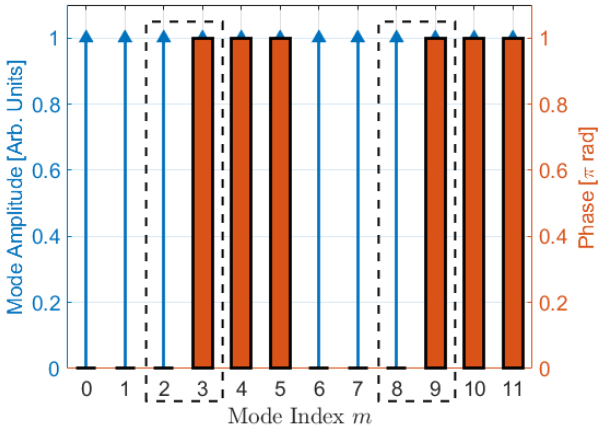

Figure 4: Ideal pulse shaper phase shifts for parallel Hadamard gates. Dashed boxes outline the logical modes.

1.3 Integrated photonics

Fiber-based optical systems can support quantum frequency processing, but there are considerable challenges. Experiments are limited by the amount of space available for components, the resolution of distinct quantum channels, and total optical loss. Current fiber-based frequency mode quantum Hadamard gates as shown in figure 5 consist of two electro-optic modulators (EOMs) and a pulse shaper, commercial devices which together introduce > 12 dB loss.[3, 4]

Advances in photonic integrated circuits offer a possibility for smaller, scalable, specialized devices and a path towards realizing a quantum advantage. Photonic integrated circuits (PICs) as shown in figure 5 offer an inherent reduction in the amount of physical space occupied by a quantum frequency processor. Whereas a fiber-based system covers optical table space on the scale of square meters, an integrated photonic counterpart takes up only a few square millimeters at most. In addition, since the field of integrated photonics builds on the established technology of integrated electronics, photonic devices have the potential to scale more cost-effectively than bulky fiber-based systems. Further, with proper tuning, PICs offer significantly lower internal optical losses compared to fiber-based optical systems. This benefit makes integrated photonics all the more important to the growth of quantum information science—where every photon counts.

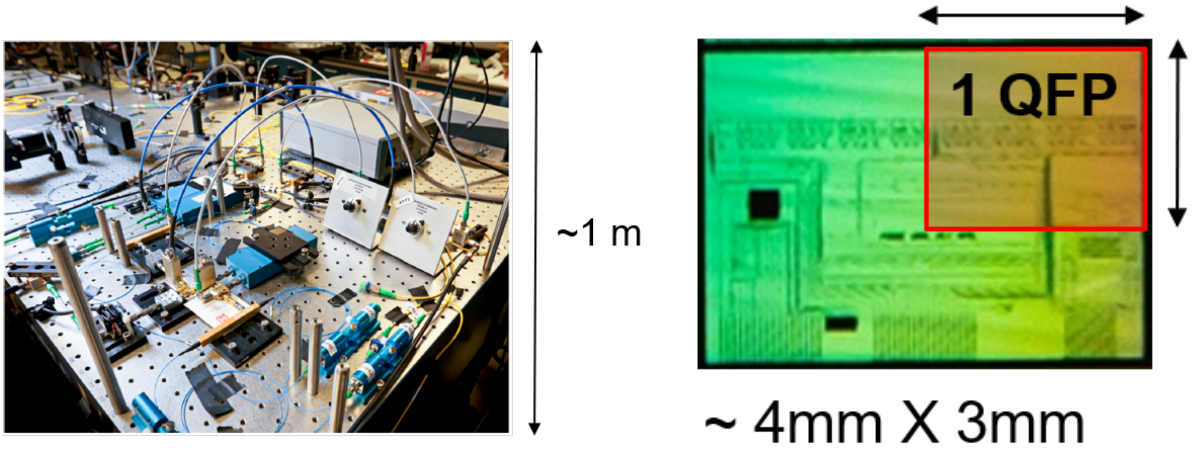

Figure 5: Left: A fiber based quantum frequency processor. Expensive commercial components filling an optical table each contribute significant loss. Right: An integrated photonic circuit on a silicon wafer. Production of these compact devices can scale, and components on chip can have low internal losses compared to bulk/fiber optics. Images courtesy of J. M. Lukens.

1.3.1 Micro-ring resonators

Micro-ring resonators (MRRs) are important components in photonic devices.[1] A simple MRR is shown in figure 6 as a pair of straight parallel waveguides[5] with an annular waveguide of radius r and round-trip length[6] $L_{\text{rt}} = 2\pi r$ positioned between them. As light propagates around this ring, it will accumulate some round trip phase $\phi = \frac{2\pi}{\lambda} n_{\text{eff}} L_{\text{rt}}$ determined by the effective index of the ring n_{eff} and the wavelength λ. It will also lose some overall amplitude $A = e^{-\alpha L_{\text{rt}}/2}$ characterized by the attenuation parameter α due to e.g. internal scattering and/or absorption. The separation

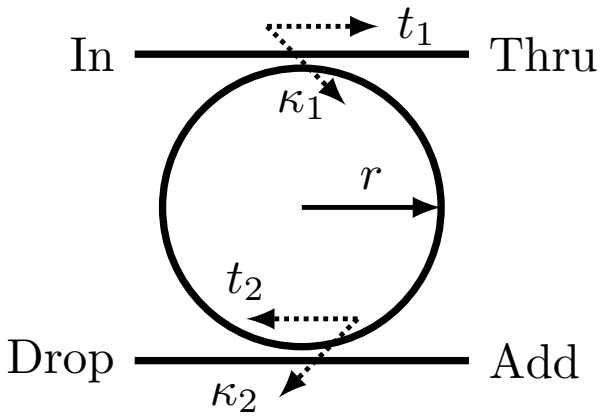

Figure 6: Schematic diagram of a photonic micro-ring resonator.

between the straight and ring waveguides determine the coupling coefficients κ_1 and t_1 at the top of figure 6, and κ_2 and t_2 at the bottom of figure 6. Since light may make several trips around the ring before coupling back out to either the drop or thru ports shown in figure 6, the full expressions for the fractions of light relative to the field at the input, summarized from Chrostowski and Hochberg [2] in equation (3), at the thru and drop ports are given by T and D respectively.

$$\begin{gathered} T \triangleq \frac{E_{\text{thru}}}{E_{\text{in}}} = \frac{t_1 - t_2 A e^{i\phi_{\text{rt}}}}{1 - t_1 t_2 A e^{i\phi_{\text{rt}}}} \qquad D \triangleq \frac{E_{\text{drop}}}{E_{\text{in}}} = \frac{-\kappa_1 \kappa_2 \sqrt{A} e^{i\phi_{\text{rt}}/2}}{1 - t_1 t_2 A e^{i\phi_{\text{rt}}}} \\ A = e^{-\alpha L_{\text{rt}}/2} \qquad \phi_{\text{rt}} = \frac{2\pi}{\lambda} n_{\text{eff}} L_{\text{rt}} \qquad L_{\text{rt}} = 2\pi r \end{gathered} \tag{3}$$

The cyclic nature of the device introduces wavelength dependent interference[7] which generates periodic resonance frequencies within the ring, and thus at the drop port of the device. Changing the radius or effective index, e.g. with an externally applied temperature or electric field gradient, changes the resonance. As such, MRRs have a wide range of applications in photonic circuits.

[5] Waveguide dimensions can vary, but are often on the order of 100s of nanometers in width and height.

[6] While the circumference on the inner and outer edges of the circular waveguide are not exactly equal, the difference is negligible for a sufficiently large ring radius relative to the width of the waveguide.

[7] Discussed at length by Bogaerts et al. [1] and Chrostowski and Hochberg [2].

1.3.2 M-mode pulse shaper on-chip

With the ability to filter out designated frequencies from an input signal, a pulse shaper as shown in figure 7 isolates a pre-defined vector of M linearly spaced frequency modes $\omega_m = \omega_0 + m\Delta\omega$. The pulse shaper then applies an arbitrary phase shift φ_m to each filtered signal ω_m. Such a device

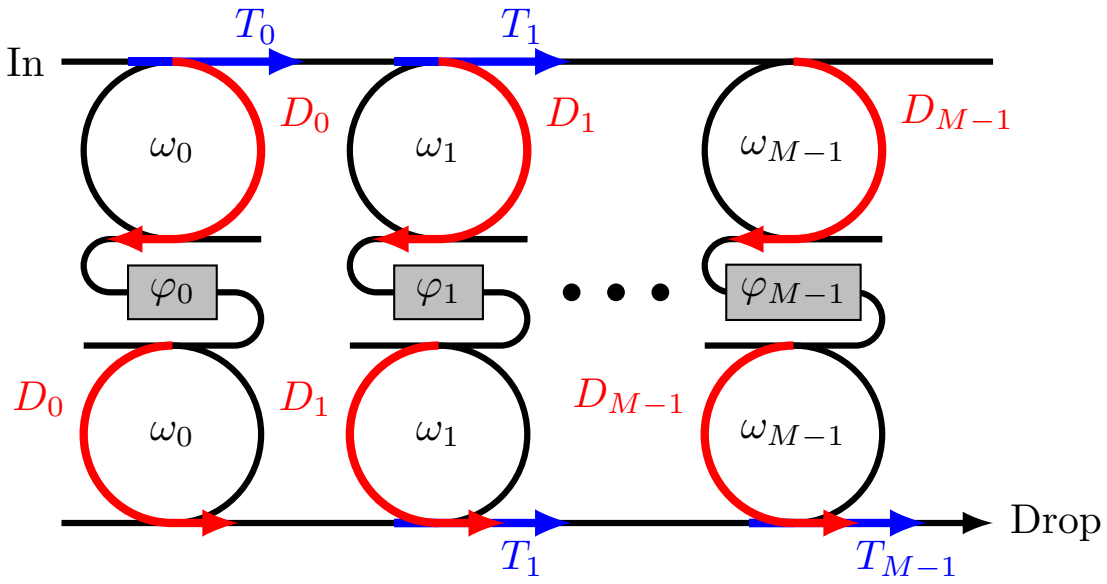

Figure 7: Schematic diagram of an M-mode pulse shaper.

will generate an output as described by equation (4), which accounts for each path light could take from the input, dropping into and out of one of the filters, and through to the output.

$$PS_{\text{drop}} = \sum_{p=0}^{M-1} \left(D_p^2 e^{i\varphi_p} \prod_{q \neq p} T_q \right) \tag{4}$$

Arbitrary per-mode phase shifts allowed us to implement quantum gates including single and parallel Hadamard gates in a Hilbert space of M frequency bins.

2 Methods

For the purpose of this thesis, it will be sufficient to assume a nominal waveguide attenuation of $\alpha = 1$ dB/cm, ring radii $r \approx 20$ μm, and symmetric coupling constants $\kappa_1^2 = \kappa_2^2 \triangleq \kappa^2 = 0.01$ for each ring in the pulse shaper. Further, $\omega_0 = 193$ THz and $\Delta\omega = 15$ GHz shall define the frequency mode space ω_m used by the pulse shaper (in the telecom band).

2.1 Fidelity calculations

As the Hadamard gate operates on general modes, it is necessary to consider quantum states at the input in order to evaluate how well the gate will perform for quantum information. For a single photon, the fidelity and success probability are calculated by comparing the target transformation H as defined in equation (1) with the mode transformation state W applied by the model. The fidelity $\mathcal{F}$ is defined [3, 4] as shown in equation (5) by the Hilbert-Schmidt inner product,

$$\mathcal{F} = \frac{\mathrm{Tr}\left(W^\dagger H\right)\mathrm{Tr}\left(H^\dagger W\right)}{\mathrm{Tr}\left(W^\dagger W\right)\mathrm{Tr}\left(H^\dagger H\right)}. \tag{5}$$

The success probability $\mathcal{P}$ is similarly calculated [3, 4] as shown in equation (6),

$$\mathcal{P} = \frac{\mathrm{Tr}\left(W^\dagger W\right)}{\mathrm{Tr}\left(H^\dagger H\right)}. \tag{6}$$

The simple case corresponds to measurements directly at the peaks of the transmitted frequency modes as shown in figure 8. To better characterize the effectiveness of the gate, the fidelity and success probability were also measured at a series of frequency offsets relative to the mode peaks.

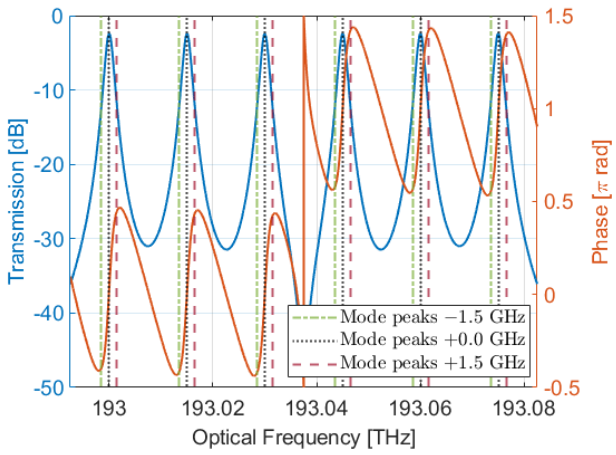

Figure 8: Pulse shaper output used to compute fidelity. ω_2 and ω_3 are 193.030 and 193.045 THz.

2.2 Log-fit to phase modulator data

Whereas figure 2 shows the ideal linear response of an EOM, recognizing and modeling the true nonlinear behavior of an EOM allows for a more realistic prediction of the effects of variable control signals upon the fidelity of the Hadamard gate. Figure 9 shows one model described by Chrostowski and Hochberg [2] for the phase shift and attenuation due to an EOM. I fit this model to a logarithmic

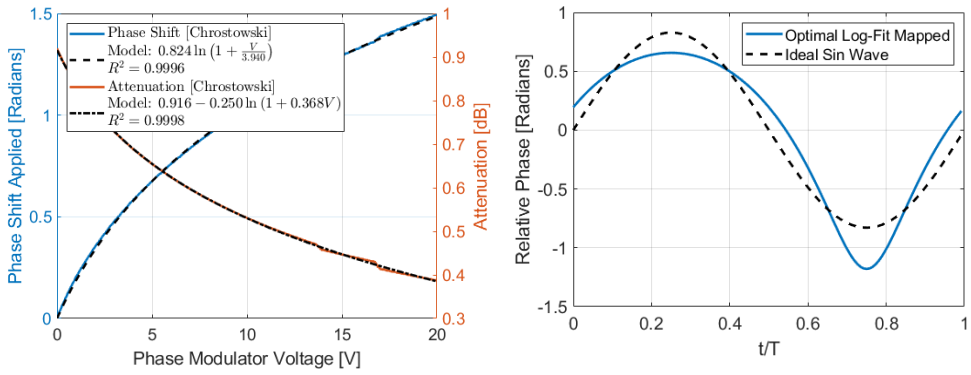

Figure 9: Left: Logarithmic fit to phase modulator data from Chrostowski and Hochberg [2]. Right: Logarithmic mapping of drive voltage period to applied phase vs. the ideal case.

function as described by equation (7a) where the drive voltage V is as indicated in equation (7b), with all other parameters being constants fit to the model.

$$\Delta\phi = a\ln\left(1+\frac{V}{V_0}\right) \tag{7a}$$

$$V = V_{\mathrm{dc}} + V_1\sin(\Delta\omega t) \tag{7b}$$

As shown in figure 10, I found the V_1 of equation (7b) for the model in figure 9 which gave the optimal fidelity via equation (5) for a series of V_{dc} values.

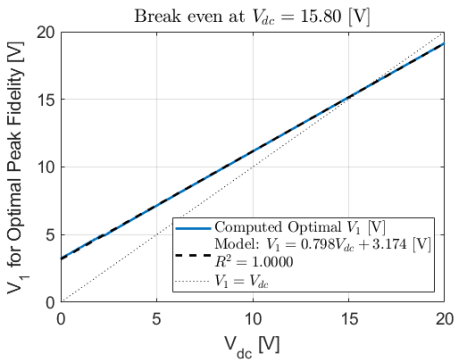

Figure 10: Dependence of V_1 on V_{dc} for optimal gate fidelity.

3 Problems and progress

It is important to note that the model described in section 2 is by no means limiting; the true model for a physical device will depend on where and how it is manufactured, as well as on various design parameters. In particular the logarithmic model for the phase modulator as described in figure 9 is also only an approximation which could potentially be adjusted to achieve better performance. Indeed, as it stands, this model poses several significant concerns, forming the basis for this thesis. In particular, I first make a minor correction to the previous code, and subsequently proceed to explore one possible route to improved fidelity.

3.1 A realistic driving voltage model

An appealing physically reasonable EOM driving voltage solution for optimal fidelity would yield low attenuation and have a voltage swing of only a few volts over each period of oscillation. As shown in figure 10, for $V_{\mathrm{dc}} < 15.8V$, $V_1 > V_{\mathrm{dc}}$, and there are points over the drive cycle where equation (7b) becomes negative, inducing very significant loss as shown in figure 9. In order to keep total voltage positive over the drive cycle, it is necessary to make $V_{\mathrm{dc}} > 15.8V$, and to maintain a low total attenuation per figure 9, V_{dc} must be even larger. I modified the code optimizing the voltage function, limiting the maximum V_1 returned for a given V_{dc} value. I allowed the V_1 to be optimized as before, but in the cases where $V_{\mathrm{dc}} > V_1$, I adjusted the code to instead return $V_1 = V_{\mathrm{dc}}$, thereby maintaining $V \geq 0$ as shown in figure 11 for the EOM driving voltage as defined in equation (7b) as desired. However, the minimum voltage for suitable fidelity is undeviated.

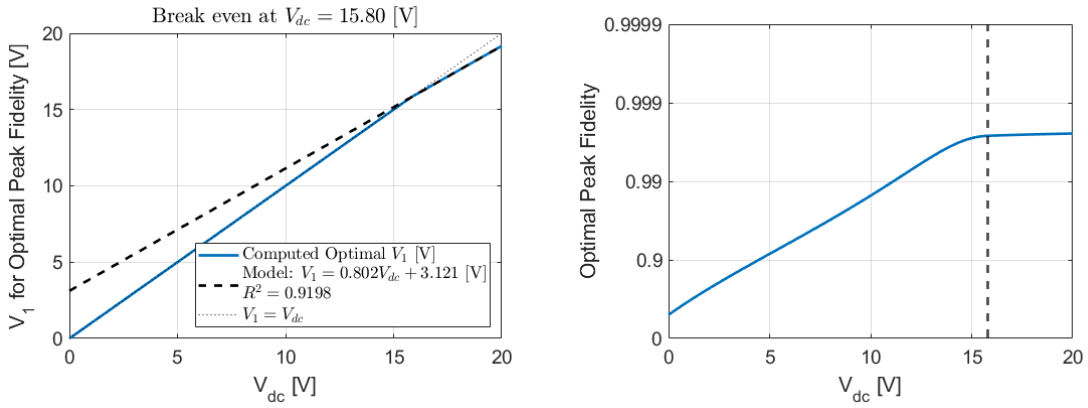

Figure 11: Left: V_1 constrained, maintaining $V \geq 0$. In this case, the model is only fit to values of V_1 which naturally want to be less than V_{dc} for optimal fidelity during the driving period. Right: Optimal fidelity for the computed optimal V_1 in the center plot. The break even voltage is identified by the dashed line. Increasing V_{dc} beyond this point does not significantly improve the fidelity.

3.2 Waveguide doping modification

There are many parameters which will need to be adjusted in this model prior to production, but as manufacturers do not typically publish details of the models they use, exploration of the space is warranted. One particular component of the model provided by Chrostowski and Hochberg [2] is the semiconductor doping of the EOM waveguide.

I implemented simple scale parameters in the code to adjust the doping densities of both the acceptor and donor materials such that setting these parameters to unity would maintain the original values set by Chrostowski and Hochberg [2]. I then swept these scale parameters logarithmically from 10^{-1} to 10^{1}. For each pair of acceptor and donor doping values as shown in figure 12, I calculated the optimal fidelity as described above in section 2, along with the appropriate V_{dc}, which then determines V_1 via a similar process to that shown in figure 11. It is important to

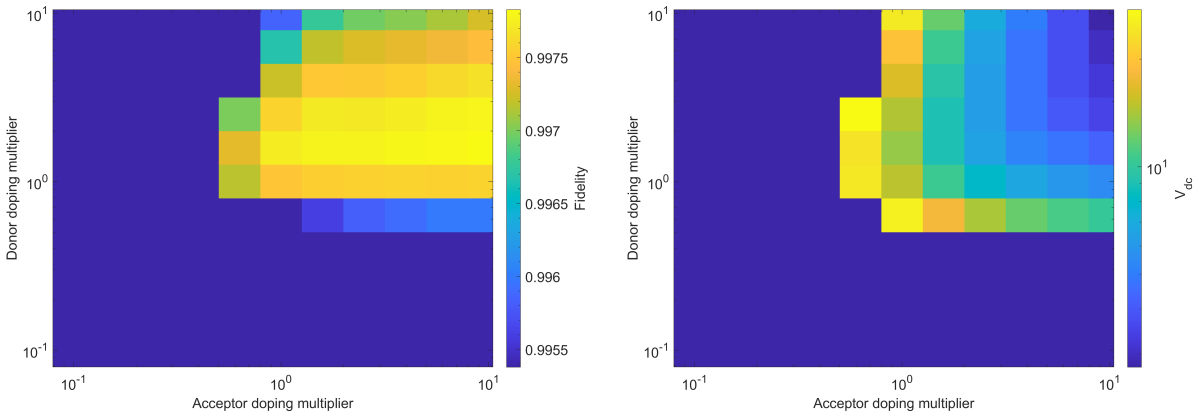

Figure 12: Parameter sweep over the semiconductor doping in the EOM waveguide relative to the values provided by Chrostowski and Hochberg [2]. Left: Optimal Hadamard gate fidelity obtained. Right: V_{dc} for EOM drive cycle used. Note that greater fidelity seems to correlate with lesser V_{dc}.

note that since these calculations were done with an ideal pulse shaping component as described in figure 4, I needed to reevaluate the system with the optimal parameters, in this case with acceptor and donor doping multipliers of about 10 and 1.6 respectively, and a V_{dc} of around 4.5 V, using the full pulse shaper model. I then compared the fidelity and success probability in figure 13 obtained via equations (5) and (6) for the original dopings provided by Chrostowski and Hochberg [2] and for the scaled doping values as found in figure 12.

Upon initial inspection of figure 13, it is evident that changing the doping has increased the gate fidelity as desired. Whereas with the original doping values the fidelity was around 0.996, with the modified doping values the fidelity is now 0.997. While certainly not a revolutionary

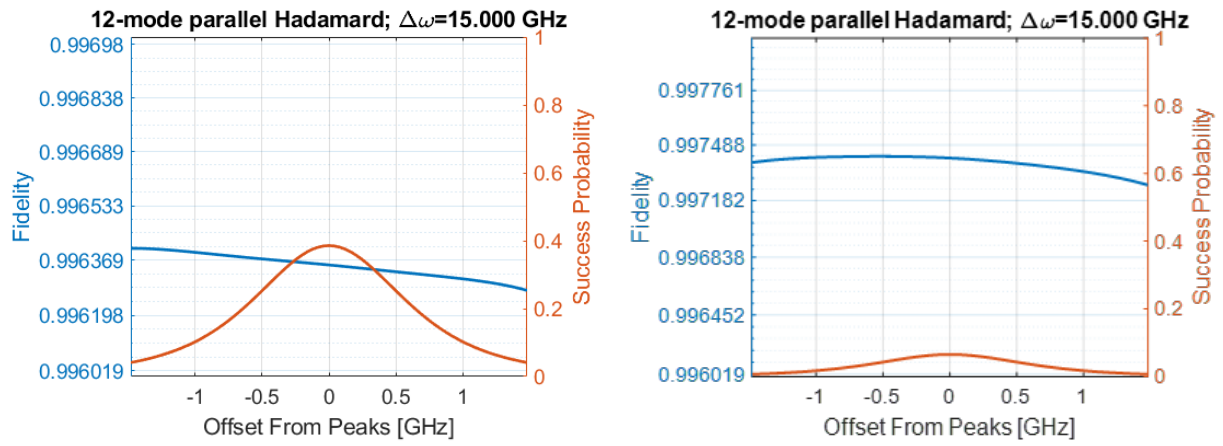

Figure 13: Comparison of Hadamard gate fidelity and success probability between the original doping (left) and modified doping (right). Changing the doping increases the fidelity at the expense of success probability.

development, this increase could be indicative of future improvement with more manipulation. However, the drop in success probability from around 0.4 to less than 0.1 is significant. Upon investigation of the full EOM response to a drive voltage, figure 14 reveals the true pitfall in modifying the doping values: whereas for a given voltage the phase shift applied by the EOM does not change significantly with the altered doping values, the attenuation increased by > 6 dB. Thus, this significant loss, likely due in practice to increased scattering and/or absorption within the

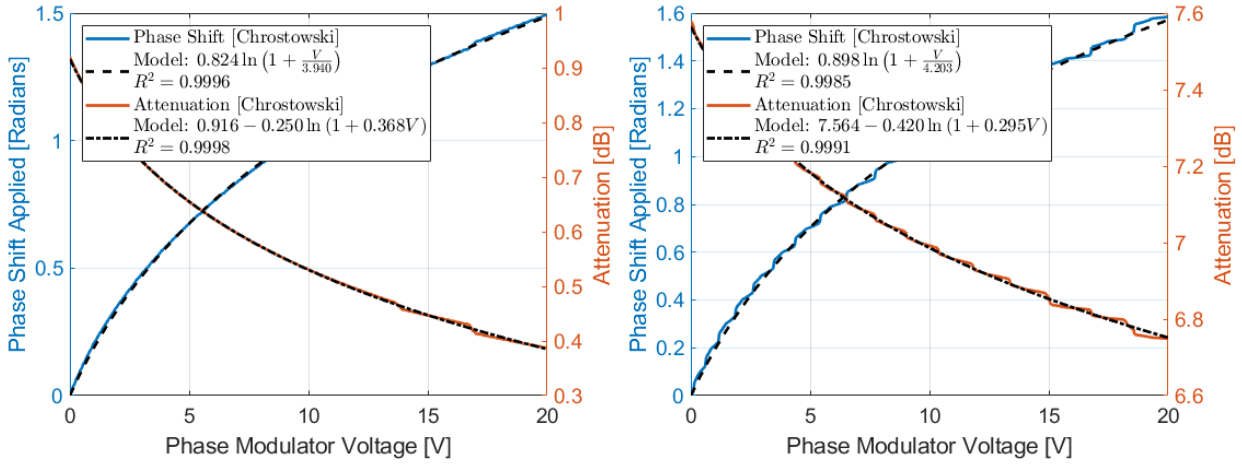

Figure 14: Comparison of EOM phase shift and attenuation response with respect to applied voltage between the original doping (left) and modified doping (right). Changing the doping introduces a significant amount of attenuation.

waveguide, prevents doping alteration alone from providing feasible and meaningful improvement to the fidelity of the Hadamard gate.

4 Conclusion

I have developed a photonic electro-optic circuit for on-chip quantum frequency processing. As photonic component design is a complex optimization problem, there is much room for further exploration; this model was one of many. Although changing the doping to improve fidelity ultimately proved unrealistic, any performance guidelines that result from this or future simulations should be considered with the caveat that manufacturers will always have their own designs.

Beyond the work described here, further modeling in software is possible, to explore what effect modifying other parameters such as the waveguide geometry might have on the fidelity of the gate. Another consideration, which Prof. W. H. Knox suggested may be more realistic than previously thought, would be to abandon the sinusoidal voltage and instead tune a nonlinear drive signal to the EOM model. Further efforts might explore other quantum gates such as the CNOT, towards developing a fully integrated quantum computer and quantum communications network.

5 Funding

This work was supported in part by the U.S. Department of Energy, Office of Science, Office of Workforce Development for Teachers and Scientists (WDTS) under the Science Undergraduate Laboratory Internship program. I developed the foundation of this project during the summer of 2020 under Dr. Joseph Lukens at Oak Ridge National Lab through the SULI program.

6 Acknowledgements

I would like to thank Dr. Joseph Lukens for his advice, encouragement, and support from when I first contacted him prior to my internship at ORNL, through the summer I was working with him, and over the duration of this thesis. I would also like to thank Dr. Nick Vamivakas for serving as my thesis advisor and for allowing me to be a research assistant in his lab since the summer of 2019. I would further like to thank S. A. Wadood for his mentorship throughout and beyond the duration of my project in the Vamivakas lab, and Hsuan-Hao Lu and Navin Lingaraju of Purdue University for their part in the foundations of this thesis developed during my internship with Dr. Lukens. In addition, I would like to thank Dr. Julie Bentley and Dr. Scott Carney for their consistently invaluable advice, for their roles in advancing my academic and professional endeavors, and for sharing with me their passion for the field of optics.

References

[1] W. Bogaerts et al. "Silicon microring resonators". In: *Laser & Photonics Reviews* 6.1 (Sept. 2011), pp. 47–73. DOI: 10.1002/lpor.201100017. URL: http://dx.doi.org/10.1002/lpor.201100017.

[2] Lukas Chrostowski and Michael Hochberg. *Silicon Photonics Design: From Devices to Systems*. 1st ed. Cambridge University Press, 2015. ISBN: 1107085454,9781107085459. URL: http://gen.lib.rus.ec/book/index.php?md5=8767cee0b433fe024e3acdb1607f54b6.

[3] Hsuan-Hao Lu et al. "Electro-Optic Frequency Beam Splitters and Tritters for High-Fidelity Photonic Quantum Information Processing". In: *Phys. Rev. Lett.* 120 (3 Jan. 2018), p. 030502. DOI: 10.1103/PhysRevLett.120.030502. URL: https://link.aps.org/doi/10.1103/PhysRevLett.120.030502.

[4] Joseph M. Lukens and Pavel Lougovski. "Frequency-encoded photonic qubits for scalable quantum information processing". In: *Optica* 4.1 (Jan. 2017), p. 8. DOI: 10.1364/optica.4.000008. URL: http://dx.doi.org/10.1364/OPTICA.4.000008.